Microbial Biotechnology

WILEY

MICROBIAL BIOTECHNOLOGY Open Access

RESEARCH ARTICLE OPEN ACCESS

A Modular Design of a Cholera Toxin B Subunit-Scaffolded Sub-Virion Nanoparticle Vaccine Against West Nile Virus

Hyun Byun[1] | Tae Hoon Kim[2] | Jemin Sung[3] | Jung-Min Lee[4] | Sang-Mu Shim[4] | Sin Hae Kang[2] | Hanul Kang[2] | Dah Hyun Moon[2] | Seong Hyun Park[5] | Doda Kim[2] | Sung Jae Kim[6,7] | Seunghoo Kim[6] | Gyoonhee Han[1,2] | Baik Lin Seong[8,9]

[1]Department of Integrated OMICS for Biomedical Science, Yonsei University, Seoul, South Korea | [2]The Interdisciplinary Graduate Program in Integrative Biotechnology, Yonsei University, Incheon, South Korea | [3]Department of Biotechnology, Yonsei University, Seoul, South Korea | [4]Division of Acute Viral Diseases, Center for Emerging Virus Research, National Institute of Health, Korea Disease Control and Prevention Agency, Cheongju, South Korea | [5]Graduate Program in Biomaterials Science and Engineering, Yonsei University, Seoul, South Korea | [6]Vaxdigm Co., Ltd., Seoul, South Korea | [7]Bio & Living Engineering Major, Yonsei University, Seoul, South Korea | [8]Department of Microbiology, Yonsei University College of Medicine, Seoul, South Korea | [9]Vaccine Innovative Technology ALliance (VITAL)-Korea, Yonsei University, Seoul, South Korea

Correspondence: Gyoonhee Han (gyoonhee@yonsei.ac.kr) | Baik Lin Seong (blseong@yonsei.ac.kr)

Received: 7 November 2025 | **Revised:** 7 May 2026 | **Accepted:** 14 May 2026

Keywords: cholera toxin B | cross-reactivity | flavivirus | sub-virion nanoparticle

ABSTRACT

Although veterinary vaccines against West Nile virus (WNV) have been developed, no approved human vaccine is currently available, highlighting the need for scalable and safer WNV vaccine candidates. In this study, a recombinant WNV subunit nanoparticle vaccine was developed by displaying the envelope protein domain III (ED3) on a cholera toxin B subunit (CTB) pentameric scaffold. The resulting recombinant protein comprising CTB-ED3 was expressed predominantly as soluble nanoparticles in *Escherichia coli*. Immunized mice produced strong humoral responses with balanced IgG1/IgG2a ratios, and some constructs achieved neutralizing titres comparable to those elicited by formalin-inactivated WNV. Importantly, no cross-reactivity with other flaviviruses was observed, alleviating potential concerns about ADE. These findings demonstrate that CTB-ED3 is assembled into multimeric nanoparticles in bacteria, offering a cost-effective, scalable, and biosafe platform for developing subunit nanoparticle vaccines against WNV and potentially other flaviviruses.

1 | Introduction

West Nile virus (WNV) is an arthropod-borne pathogen that poses a significant threat to human health and can cause severe health conditions (Mukhopadhyay et al. 2003, Kanai et al. 2006, Brinton 2014). It is a single-stranded RNA virus belonging to the family *Flaviviridae*, genus *Flavivirus*, which also includes Dengue virus (DENV), Zika virus (ZIKV), and Japanese encephalitis virus (JEV) (Lindenbach and Rice 2003; Mukhopadhyay et al. 2005). Although WNV vaccines have been developed for veterinary use, there are currently none available for human application. The development of human WNV vaccines has been hindered largely by difficulties in conducting efficacy trials, as WNV outbreaks occur sporadically and unpredictably, making it challenging to recruit sufficient participants for large-scale clinical studies (Kaiser and Barrett 2019; Gould et al. 2023). In addition, the relatively limited market size has reduced incentives for vaccine development (Curren et al. 2021; Gould et al. 2023). Therefore, the development of an effective and safe human WNV vaccine remains an important public health priority. In flavivirus infections, antibody-dependent enhancement (ADE) has been reported in vitro when non-neutralizing or sub-neutralizing antibodies facilitate viral entry into host cells (Thomas

Hyun Byun and Tae Hoon Kim contributed equally to this work.

et al. 2022). Notably, WNV has demonstrated potential cross-reactivity that leads to ADE in the context of previous ZIKV infection, likely due to structural similarities between the viruses (Bardina et al. 2017). This highlights the importance of eliciting the production of specific neutralizing antibodies. One promising strategy involves designing subunit vaccines that target the WNV envelope protein domain III (ED3), which is known to induce strong neutralizing antibody responses while avoiding ADE-associated regions (Thomas et al. 2022). Subunit vaccines are emerging as a promising option because of their ability to offer high immunogenicity while addressing safety concerns associated with other vaccine types (Moyle and Toth 2013; de Pinho Favaro et al. 2022). Therefore, a novel design of the WNV sub-virion vaccine that preferably targets protective epitopes and minimizes the ADE risk would provide a safe option for effective protection from infection.

A flavivirus particle is characterized by a spherical structure enveloped in a lipid bilayer that is derived from the host cell membrane. The key components of this viral envelope include envelope (E) and membrane (M) glycoproteins, with the E protein playing a crucial role in viral attachment and fusion with host cells (Kuhn et al. 2002; Stiasny et al. 2007; Heinz and Stiasny 2012; Zhao et al. 2021). The E protein consists of three domains: ED1, ED2, and ED3 (Heinz and Stiasny 2012). Notably, in the case of WNV, considerable focus of vaccine development centers on the ED3 region. This domain is crucial for receptor binding and facilitates the virus's attachment and entry into host cells (Rey et al. 1995; Chu et al. 2005). In contrast, ED2 contains a highly conserved fusion loop that often induces cross-reactive but poorly neutralizing antibodies, which have been implicated in ADE during subsequent flavivirus infections (Flores et al. 2025). Consequently, targeting the ED3 region in vaccine design aims to elicit an immune response that effectively neutralizes the virus, thereby preventing its ability to infect cells and providing a foundation for protective immunity against WNV infection. Moreover, ED3-specific antibodies are generally WNV-specific and potently neutralizing, with a lower propensity to mediate ADE, thus making ED3 a safer and more reliable antigenic target for subunit vaccine strategies (Crill and Roehrig 2001; Chu et al. 2005; Sun et al. 2023). Nevertheless, because ED3 is a relatively small domain, its immunogenicity can be further enhanced by presenting the antigen in a repetitive structural arrangement, which promotes efficient B cell receptor cross-linking and antigen presentation (Bachmann and Jennings 2010; Spohn et al. 2010; Zlatkovic et al. 2011). On the viral surface, five ED3 units from neighbouring E proteins are arranged around the fivefold axis, forming a pentameric configuration (Zhang et al. 2004). To enhance immunogenicity, the cholera toxin B subunit (CTB) was employed as a pentameric scaffold to present ED3 in a spatially organized arrangement. This design strategy aimed to preserve conformational epitopes critical for neutralization while maintaining the safety advantages of an ED3-based subunit vaccine.

Cholera toxin (CT) is secreted by *Vibrio cholerae* and is a major virulence factor responsible for the severe diarrheal symptoms of cholera (Holmgren and Lönnroth 1973; Gill and Rappaport 1979; Sanchez and Holmgren 2005). CT is composed of two subunits: the enzymatically active A subunit (CTA; 28 kDa), which catalyses ADP-ribosylation of the host G proteins and disrupts adenylate cyclase signalling, and the non-toxic B subunit (CTB; 11.6 kDa), which forms a homopentamer that binds to GM1 ganglioside receptors on the host cell surface (Hardy et al. 1988; Wernick et al. 2010; Stratmann 2015). While CTA is responsible for the pathological effects of cholera, CTB facilitates the uptake of the holotoxin across mucosal surfaces without inducing toxicity (Stratmann 2015). Because of its stable pentameric structure composed of five noncovalently associated identical subunits and its strong affinity for GM1, CTB has emerged as an effective scaffold for vaccine development (Baldauf et al. 2015; Ahn et al. 2023). It functions as an antigen delivery system and immunomodulatory agent, capable of enhancing mucosal and systemic immune responses when conjugated or fused with target antigens (George-Chandy et al. 2001; Stratmann 2015). These properties, including low toxicity, robust mucosal immunogenicity, and efficient antigen presentation, have positioned CTB as a mucosal adjuvant and scaffold for subunit vaccine research against various infectious diseases (George-Chandy et al. 2001; Baldauf et al. 2015).

In this study, we designed a recombinant WNV sub-virion nanoparticle by genetically fusing ED3 to CTB. To facilitate recombinant protein production in *E. coli*, fusion tags were incorporated into the constructs. The expression, assembly, and antigenic properties of the recombinant CTB–ED3 constructs were evaluated to explore their potential as a sub-virion nanoparticle vaccine candidate against WNV. Immunization with the recombinant antigen induced virus-neutralizing antibodies in mice, supporting the potential of this approach for WNV vaccine development.

2 | Material and Methods

2.1 | Design of the Plasmids

A schematic presentation of the tripartite constructs, comprising a fusion tag, pentameric scaffold (CTB), and the WNV EDIII antigen, is shown in Figure 1a. Genes encoding CTB (GenBank: HAS3667523.1) and WNV ED3 (GenBank: ADD23612.1) were synthesized using *E. coli* codon optimization (Bionics Co. Ltd., Korea). In addition, two mutant CTBs (C9S and Y12D) were synthesized. These genes were then digested and inserted into modified pGE-fusion tag expression vectors derived from pGEMEX-1 (Promega, USA). Three laboratory-developed fusion tags were used: NC (nucleocapsid protein from HIV-1 Gag polyprotein (Mouhand et al. 2020)), AsnRS (N-terminal domain of the yeast asparaginyl tRNA synthetase (Kern et al. 2013)), and hRID (N-terminal domain of human lysyl tRNA synthetase (Kwon et al. 2018)). Each fusion tag contained a TEV recognition sequence, a 6× His tag, and *Kpn*I-*BamH*I-*Eco*RV-*Hind*III restriction sites, followed by the CTB and WNV ED3 inserts. Specifically, CTB and mutant CTBs were inserted into the *Kpn*I-*BamH*I restricted site, while WNV ED3 was placed within the *BamH*I-*Eco*RV restricted site. The plasmid constructs comprising a fusion tag, CTB, and WNV ED3, along with variations of the mutant CTBs (C9S and Y12D) are also shown in Figure 1b. The predicted molecular weights of all recombinant constructs, including their monomeric and pentameric forms before and after TEV cleavage, are summarized in Table 1.

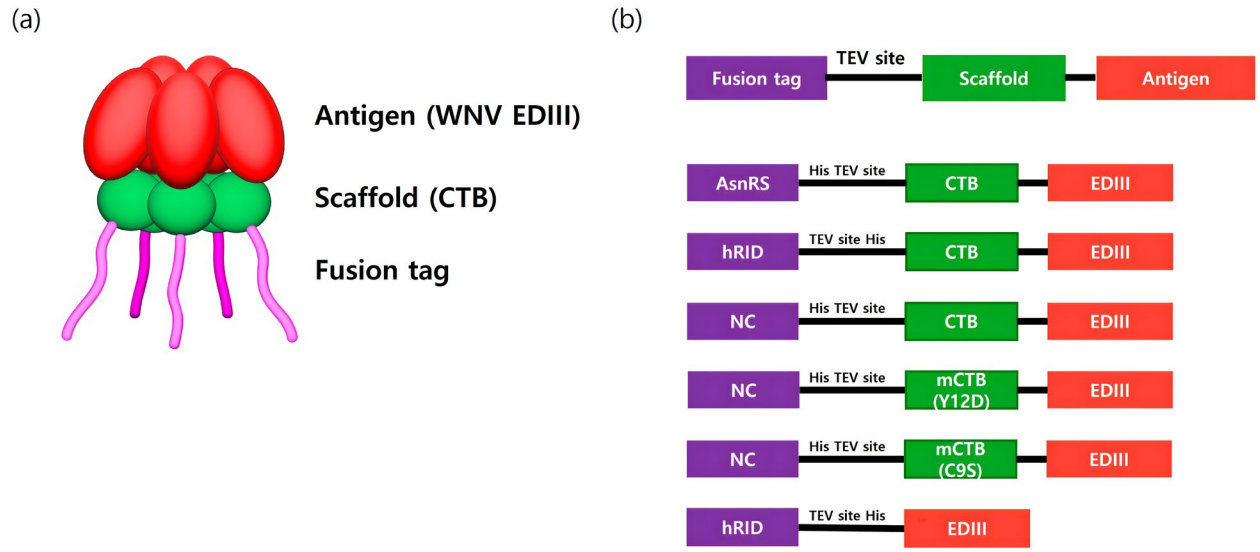

FIGURE 1 | Plasmid constructs with detailed genome components. (a) Schematic illustration of the tripartite constructs, comprising the fusion tag, the scaffold (CTB), and the WNV ED3 antigen. (b) Each construct, except for hRID-ED3, included a fusion tag, either CTB or a mutated form of CTB, fused to WNV ED3 at the C-terminus. TEV cleavage sites were inserted between the fusion tag and CTB to allow the removal of the fusion tag if necessary.

TABLE 1 | Predicted molecular weights of recombinant antigens in monomeric and pentameric forms before and after TEV cleavage.

Construct	TEV cleavage	Monomer (kDa)	Pentamer (kDa)
AsnRS–CTB–ED3	–	35.4	177
(AsnRS) CTB–ED3	+	24	120
hRID–CTB–ED3	–	32.5	162.5
(hRID) CTB–ED3	+	24	120
NC–CTB–ED3	–	30.8	154
(NC) CTB–ED3	+	24	120
(NC) mCTB(Y12D)–ED3	+	24	120
(NC) mCTB(C9S)–ED3	+	24	
(hRID) ED3	+	10.8	

Note: Predicted molecular weights (MW) of recombinant antigen constructs are presented for both monomeric and pentameric forms, before (–) and after (+) TEV protease cleavage. Pentameric MW values were calculated based on the assumption of a homopentameric assembly of the monomer units.

2.2 | Protein Expression and Purification

Transformed *E. coli* SHuffle cells (New England Biolabs, USA; cat no. C3026J) were inoculated into 3 mL of Luria-Bertani (LB) medium containing ampicillin (50 μg/mL) and incubated overnight at 30°C. Thereafter, 3 mL of the cell culture was transferred to 20 mL of fresh LB medium with the same antibiotics and cultured at 30°C until the optical density (OD) reached 0.6–1.0. Once the OD was within the optimal range, 20 mL of cell culture was divided into 6 mL portions for induction and non-induction purposes. Subsequently, 1 mM IPTG was added to only the induction culture, and the cells were incubated overnight at 20°C. After incubation, 5 mL of the cell culture was harvested by centrifugation. The harvested cells were resuspended in lysis buffer [50 mM Tris–HCl (pH 7.5), 300 mM NaCl, 10% glycerol, 10 mM imidazole, 0.1% Tween-20, and 2 mM 2-mercaptoethanol] and lysed by sonication. The total cell lysates were separated into soluble and pellet fractions by centrifugation at 18,214 *g* for 10 min. The total, soluble, and pellet fractions were analysed by SDS-PAGE. Additionally, SDS-PAGE was performed under non-reducing conditions to provide indirect evidence for the assembly of CTB-fused recombinant proteins.

For large-scale laboratory culture, transformed *E. coli* SHuffle cells were cultured in 1 L of LB medium under the same conditions as described above. The harvested cells were lysed by sonication in 20 mL of lysis buffer. The resulting supernatant was loaded onto an EconoFit Nuvia IMAC column (Bio-Rad, USA) using a Biologic LP system (Bio-Rad) for affinity purification. After equilibration with lysis buffer (10 mM imidazole), protein elution was performed using a linear gradient of buffer B (300 mM imidazole). For hRID- and AsnRS-fused proteins, elution was carried out using a 10%–100% buffer B gradient, whereas for NC-fused proteins, a 20%–100% buffer B gradient was applied. Fractions containing the target proteins were identified by SDS-PAGE analysis and subsequently collected. These fractions were dialyzed in a storage buffer containing 50 mM Tris–HCl (pH 7.5), 300 mM NaCl, and 2 mM EDTA. Finally, the purified proteins were concentrated using an Amicon 10 K filter (Merck, Germany; cat no. UFC9010). Following Ni-affinity purification, the samples were further purified by size exclusion chromatography (SEC) using the NGC system (Bio-Rad). For TEV cleavage, TEV protease (Invitrogen, USA; cat no. 12575015) was applied for 3 days at 4°C. Untreated samples were analyzed in parallel. The Superdex 200 column (GE Healthcare, Sweden) was equilibrated with a buffer consisting of 50 mM Tris-Cl (pH 7.5) and 300 mM NaCl. Subsequently, the Ni-affinity purified samples were loaded onto the column, and the samples were eluted at a rate of 0.3 mL/min. The eluted samples were then analyzed by SDS-PAGE.

2.3 | GM1 Binding Assay

GM1 (Biosynth, Switzerland; cat no. OG03918) was diluted in a carbonate–bicarbonate buffer (pH 9.6) to a concentration of 3 μg/mL. Following this, 100 μL of the GM1 solution was added to each well of an immunoassay plate (Thermo Fisher Scientific; cat no. 439454), followed by overnight incubation. After washing the plate three times with phosphate-buffered saline with Tween-20 (PBST) (PBS, Gibco; 0.05% Tween-20, Merck, Germany), each well was blocked with 200 μL of 1% bovine serum albumin (BSA) for 2 h at room temperature (RT). After blocking, the plate was washed with PBST three times. Serially diluted samples, including SEC-purified recombinant proteins and commercial CTB (Sigma-Aldrich, USA; cat no. SAE0069) initially adjusted to 18.75 nM, were added to the wells, and the plate was incubated for 4 h at RT. After a triple PBST wash, 100 μL of anti-CTB mouse serum (1:2,000 dilution) was added to each well and incubated for 1 h at RT, followed by another PBST wash. Subsequently, 100 μL of anti-mouse IgG H + L (1:10,000 dilution; BETHYL, USA; cat no. A90-116P) antibody was added to each well and incubated for 1 h at RT, followed by another PBST wash. For colour development, 100 μL of TMB (BD Biosciences, USA; cat no. 555214) was added to each well and incubated for 30 min at RT, and the reaction was stopped by adding 50 μL of 2 N H_2SO_4. The OD intensity of each well was measured using an absorbance plate reader (BMG LABTECH, Germany).

2.4 | E24-Binding ELISA

To assess the structural integrity of WNV ED3, an ELISA was performed using the monoclonal antibody E24 (ATCC, USA; cat no. VR-1612) which recognizes the lateral ridge epitope of WNV ED3 (Oliphant et al. 2005, 2006). Each antigen was coated onto an immunoassay plate (Thermo Fisher Scientific) at a concentration of 0.1 μg/well and incubated overnight at 4°C. Commercial recombinant WNV E protein (Abcam, England; cat no. ab256449) was included as a positive control. The plate was then blocked with 1% BSA for 2 h at RT. Subsequently, 100 μL of the E24 monoclonal antibody, initially diluted 1:1,000 and subjected to 5-fold serial dilutions, was added to each well. After incubation for 1 h at RT, 100 μL of anti-mouse IgG H + L antibody (BETHYL) diluted 1:10,000 was added to each well and incubated for an additional 1 h at RT. The wells were then treated with 100 μL of TMB solution and incubated for 30 min at RT. The reaction was stopped by adding 50 μL of 2 N H_2SO_4, and the absorbance was measured using a microplate reader (BMG LABTECH).

2.5 | Transmission Electron Microscopy

For transmission electron microscopy (TEM), the SEC-purified samples were applied to a Formvar-coated 200 mesh copper grid (Electron Microscopy Sciences, USA; cat no. 71150) for approximately 1 min. The samples were then removed, blotted with filter paper, and a drop of 1% phosphotungstic acid was placed on the grid for negative staining. The excess staining solution was removed, and the grids were examined under TEM (JEM-2100Plus and JEM-F200, JEOL, Japan).

2.6 | Mouse Immunization

Five-week-old female BALB/c mice (Orient Bio, Korea) were immunized with 25 μg of various antigens as follows: AsnRS-CTB-ED3, hRID-CTB-ED3, NC-CTB-ED3, (AsnRS) CTB-ED3 (TEV-cleaved from AsnRS-CTB-ED3), (hRID) CTB-ED3 (TEV-cleaved from hRID-CTB-ED3), (NC) CTB-ED3 (TEV-cleaved from NC-CTB-ED3), (NC) mCTB(Y12D)-ED3 (TEV-cleaved from NC-mCTB(Y12D)-ED3), (NC) mCTB(C9S)-ED3 (TEV-cleaved from NC-mCTB(C9S)-ED3), and (hRID) ED3 (TEV-cleaved from hRID-ED3), each containing alum (Invivogen, USA; cat no. vac-alu-250) as an adjuvant. Negative control mice were injected with PBS adjuvanted with alum. Each group consisted of five mice and each mouse received three doses, administered intraperitoneally every 2 weeks during the six-week experimental period. Blood was collected via eye bleeding thrice every 2 weeks after the first injection, and the mice were sacrificed following the third blood collection for further analysis. All animal studies were performed under the guidelines of the Institutional Animal Care and Use Committee (IACUC) of the International Vaccine Institute (IVI) (IACUC PN 2022–006).

2.7 | ELISA Analysis

ELISA was used to measure the WNV antibody titre. First, commercial recombinant WNV E protein (Abcam) was coated onto an immunoassay plate (Thermo Fisher Scientific) at a concentration of 0.1 μg/well overnight at 4°C. The coated plates were washed three times with PBST and blocked using 200 μL of 1% BSA for 2 h at RT. Thereafter, pooled serum from each group collected from the third immunization was diluted as follows: for total IgG and IgG1, sera were initially diluted 1:800; for IgG2a, sera were initially diluted 1:100. All samples were then serially diluted fivefold using a serum dilution buffer (PBST containing 0.25% BSA) and incubated in the coated wells for 1 h at RT. After washing, a secondary antibody (1:10,000 diluted) HRP-conjugated anti-mouse IgG (BETHYL) or IgG1 (BETHYL; cat no. A90-105P) or IgG2a (BETHYL; cat no. A90-107P) was applied to the washed plates and incubated for 1 h at RT. Finally, 100 μL of TMB solution (BD Biosciences) was added to each well and incubated for 30 min, and the reaction was stopped by adding 50 μL of 2 N H_2SO_4. The OD intensity of each well was measured using an absorbance plate reader (BMG LABTECH). Endpoint titres were defined as the dilution factor (x-value) at which the fitted curve of each sample intersected with twice the OD value of the PBS group. The trendlines were generated using GraphPad Prism with the following equation: $Y = \text{Bottom} + (\text{Top} - \text{Bottom}) / [1 + 10^{((\text{LogEC50} - X) \times \text{HillSlope})}]$. All experiments were performed in triplicate.

2.8 | Neutralization Assay

The neutralization assay was performed using the infectious WNV in the BSL-3 facility of the Korea Disease Control and Prevention Agency (KDCA) located in Osong City, Korea. BHK-21 cells were prepared in 12-well plates at a concentration of 3×10^5 cells/well for the neutralization assay. The sera were inactivated by heating at 56°C for 30 min. Subsequently,

the inactivated sera were diluted 4-fold with minimum essential medium (MEM) containing 2% fetal bovine serum (FBS) and 1% penicillin–streptomycin, followed by further serial twofold dilutions. The WNV (lineage 2, B956) was diluted to a 6×10^3 PFU/mL. The serially diluted sera were then combined with the virus at a concentration of 50 PFU/120 μL. The virus-sera mixture was then incubated for 1 h in a CO_2 incubator. Following the incubation, BHK-21 cells were treated with 200 μL of the virus-sera mixture and further incubated in a CO_2 incubator for 1 h. After incubation, the supernatant was removed from the cells, and 1 mL of overlay media (4% FBS MEM (2×) and 1.5% agar in a 1:1 ratio) was added to the cells. The agar-overlaid plates were then incubated in a CO_2 incubator for 3 days. The cells were fixed with a 4% formaldehyde solution, after which the overlaid agar was carefully removed and subsequently stained with crystal violet. For comparison, plaque reduction neutralization test (PRNT) data from mice immunized with a formalin-inactivated WNV vaccine, prepared according to previously reported protocols, were provided by the KDCA (Posadas-Herrera et al. 2010; Brandler and Tangy 2013).

2.9 | Analysis of Cross-Reactivity

The potential cross-reactivity among the flaviviruses (DENV, JEV, and ZIKV) was analyzed. DENV and JEV were propagated in Vero cells as previously described (Ahn et al. 2023; Sung et al. 2024). For ZIKV propagation, Vero cells at ~90% confluency were infected at a 0.02 multiplicity of infection. After 3 h of incubation at 37°C, the inoculum was removed and replaced with fresh maintenance medium. The cultures were incubated for 3 days, after which the supernatant was collected and titrated using the plaque assay. Plaques were visualized by fixing with 4% formaldehyde and staining with 0.1% crystal violet.

For ELISA-based cross-reactivity analysis, DENV, JEV, and ZIKV were coated onto an immunoassay plate (Thermo Fisher Scientific) at a concentration of 1×10^5 PFU/well. Due to the BSL-3 restrictions associated with WNV, inactivated WNV was used and coated at a concentration of 0.1, 0.5, and 1 μg/well. Subsequent ELISA procedures were performed as described above. Briefly, after blocking for 2 h at RT, pooled mouse serum samples from each group were diluted 1:100, followed by five-fold serial dilutions, and applied to the wells. Thereafter, HRP-conjugated goat anti-mouse IgG (H + L) secondary antibody (diluted 1:10,000) was added. Following incubation, TMB substrate solution (BD Biosciences) was added to each well, and the reaction was stopped by the addition of 2 N H_2SO_4. The OD intensity of each well was measured using an absorbance plate reader (BMG LABTECH). All experiments were performed in triplicate.

2.10 | Statistical Analysis

Statistical analyses were performed using GraphPad Prism software (version 10.2.3; San Diego, CA, USA). Multiple group comparisons were analysed by one-way ANOVA followed by either Tukey's or Dunnett's multiple comparisons test, depending on the experimental design. A p-value < 0.05 was considered statistically significant (*, # $p < 0.05$; **, ## $p < 0.01$; ***, ### $p < 0.001$).

3 | Results

3.1 | Design of CTB-ED3 Antigens

To enhance the expression of viral antigens and prevent potential ADE, we used ED3 (10.8 kDa) instead of the full-size E protein (53 kDa) as the vaccine antigen. To spatially arrange ED3, CTB was employed as a pentameric scaffold to present ED3. Laboratory-developed fusion tags were incorporated into the CTB-ED3 constructs to facilitate recombinant protein production. Three variants (hRID, AsnRS, and NC) were used for comparative evaluation (Figure 1b). In addition, we designed three structural variants: Y12D mutant CTB, which retains pentamer formation but lacks receptor-binding ability; C9S mutant CTB, which is incapable of forming a pentamer (Jobling and Holmes 2002; Sung et al. 2024); and ED3 without CTB (Figure 1b). The fusion tag variants (hRID, AsnRS, and NC) and structural variants (mCTB and constructs lacking CTB) were systematically compared to evaluate recombinant antigen production and the contribution of nanoparticle formation to vaccine efficacy. For the mCTB variants, all three fusion tags were initially evaluated for expression, and the NC-tagged construct was selected for further analysis due to its relatively higher expression level (Figure S1a–c). In the case of the ED3-only construct, hRID was selected as the fusion tag because it provided sufficient soluble expression. Structural models of the designed recombinant proteins were predicted using AlphaFold 3 to visualize their overall structural features (Figure S2a–f).

3.2 | Protein Expression and Purification

Recombinant antigen proteins were induced using 1 mM IPTG to qualitatively assess the overall expression and solubility patterns of each construct. As shown in Figure 2, their expression levels increased upon induction compared with those under the non-induced conditions (Figure 2a–f). The total extract (T) was fractionated by centrifugation to yield the soluble (S) and insoluble pellet (P) fractions. All recombinant antigen proteins, including bipartite fusion constructs (Figure 2f) and tripartite fusion constructs (Figure 2a–e), exhibited solubility (40%–60%) at 20°C (Figure 2g). Under non-reducing conditions (without boiling and DTT), the monomeric-sized band (red box) disappeared, and a higher molecular weight band, consistent with oligomeric assembly, was observed instead (green box) (Figure 2a–d, S′ lane). These results suggest that the soluble monomer proteins likely assembled into a stable oligomer.

To further investigate the influence of CTB on the pentamer formation of recombinant antigen proteins, mCTB variants and ED3 without CTB were introduced. The Y12D mCTB can form pentamers but is unable to bind the GM1 receptor, whereas the C9S mCTB cannot form pentamers (Jobling and Holmes 2002). In Figure 2d,e, both mCTB variants exhibited increased expression

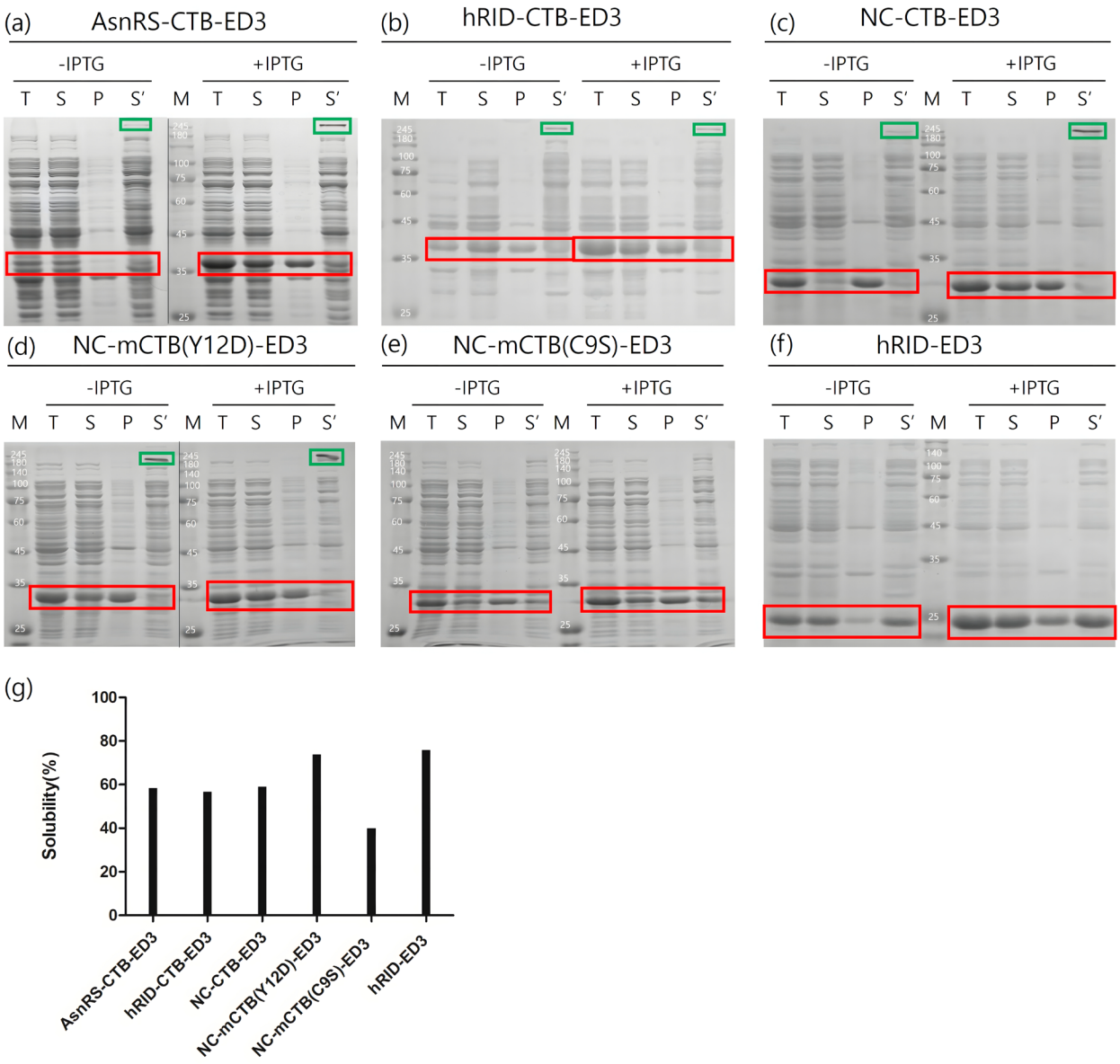

FIGURE 2 | Expression and solubility analysis of recombinant antigens in *Escherichia coli*. Coomassie blue-stained SDS-PAGE analysis of (a) AsnRS-CTB-ED3, (b) hRID-CTB-ED3, (c) NC-CTB-ED3, (d) NC-mCTB(Y12D)-ED3, (e) NC-mCTB(C9S)-ED3, and (f) hRID-ED3 expressed in *E. coli*. Recombinant antigens were expressed with and without IPTG induction to assess the expression levels and solubility. Red boxes indicate bands corresponding to the monomeric form of the recombinant antigens, while green boxes indicate bands corresponding to the oligomeric form. Lane M, marker; T, total cell lysate; S, soluble fraction of total lysate after centrifugation; P, pellet fraction of total cell lysate after centrifugation; and S′, soluble fraction of total lysate after centrifugation under non-reducing conditions without DTT and boiling. (g) Solubility index.

of soluble proteins under induction conditions compared with that under non-induction conditions. For NC-mCTB(Y12D)-ED3, the monomer band shifted to a higher molecular weight band under non-reducing conditions, which was expected. In contrast, NC-mCTB(C9S)-ED3 and hRID-ED3 without the CTB-based scaffold did not show a shift to higher molecular weight bands, as their monomer bands remained unchanged under non-reducing conditions. These findings support the role of CTB as a pentameric scaffold and its contribution to the assembly of recombinant antigens. After the initial confirmation of the solubility, each construct was purified utilizing Ni-affinity chromatography. All recombinant antigen proteins were successfully purified using Ni-affinity chromatography (Figure S3a–f).

3.3 | SEC and DLS Analysis

SEC analysis revealed three distinct peaks: peak 1 representing soluble aggregation, peak 2 the pentameric form, and peak 3 the monomeric form, as determined by calibration with molecular weight standards (Figure 3, Figure S4). Notably, for the non-TEV-treated constructs, peak 2 eluted closer to ferritin (440 kDa) than to aldolase (158 kDa) on the SEC profile. This earlier elution may be attributed to the flexible or partially disordered regions within the fusion tags, which can increase the hydrodynamic size of the proteins in solution and thereby shift their elution behaviour toward that of larger globular proteins (Some et al. 2019; Maiti et al. 2024). Protein yields following SEC purification are summarized in

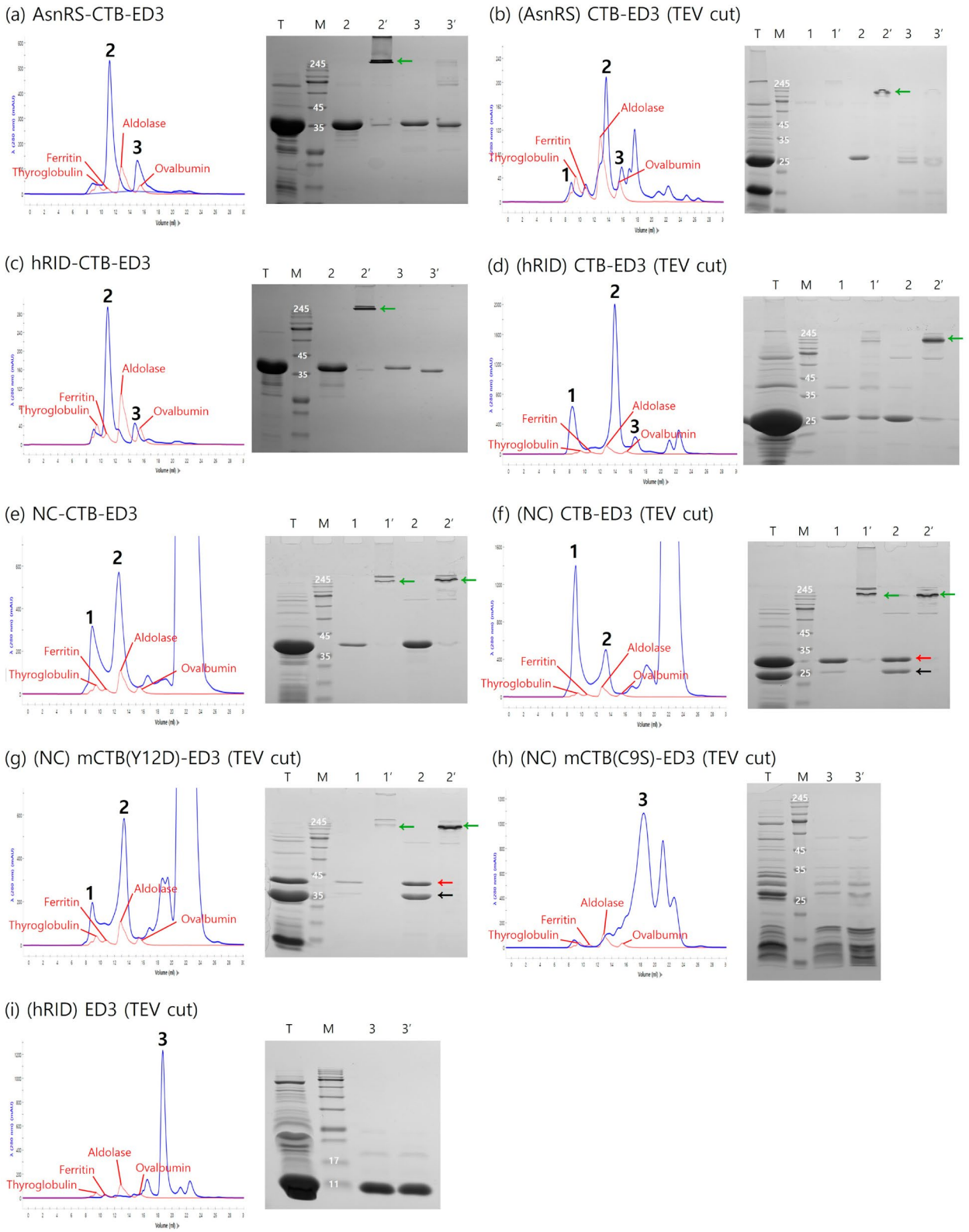

FIGURE 3 | Size exclusion chromatography analysis of the bacterially produced recombinant antigens. Size exclusion chromatography profiles of (a) AsnRS-CTB-ED3, (b) (AsnRS) CTB-ED3 after TEV cleavage, (c) hRID-CTB-ED3, (d) (hRID) CTB-ED3 after TEV cleavage, (e) NC-CTB-ED3, (f) (NC) CTB-ED3 after TEV cleavage, (g) (NC) mCTB(Y12D)-ED3 after TEV cleavage, (h) (NC) mCTB(C9S)-ED3 after TEV cleavage, and (i) (hRID) ED3 after TEV cleavage are shown. The left panel shows the absorbance at 280 nm across the elution volume. The blue line represents the sample absorbance (OD), while the red line indicates the calibration curve. The calibration markers, eluting in order from left to right, were thyroglobulin (660 kDa), ferritin (440 kDa), aldolase (158 kDa), and ovalbumin (43 kDa). The right panel shows the SDS-PAGE analysis of the selected fractions. T, total protein after IMAC; M, molecular weight marker; number, fraction number; number', fraction under non-reducing conditions without DTT and boiling. Green arrows indicate oligomer bands; black arrows, uncleaved proteins after TEV treatment; and red arrows, cleaved products.

TABLE 2 | Yield of recombinant antigens after SEC purification.

Construct	TEV cleavage	Yield (mg/1 L cell culture)
AsnRS–CTB–ED3	−	23.6
(AsnRS) CTB–ED3	+	12.6
hRID–CTB–ED3	−	22.7
(hRID) CTB–ED3	+	12.9
NC–CTB–ED3	−	5.9
(NC) CTB–ED3	+	3.8
(NC) mCTB(Y12D)–ED3	+	6.7
(NC) mCTB(C9S)–ED3	+	0.23
(hRID) ED3	+	52.9

Note: Yields of recombinant antigen constructs following size-exclusion chromatography (SEC) purification are presented as milligrams of protein obtained per litre of cell culture.

TABLE 3 | Particle size (nm) and PDI values determined by DLS.

	Construct	TEV cleavage	Size (nm)	PDI
1	AsnRS–CTB–ED3	−	12.6 ± 0.54	0.266 ± 0.028
2	(AsnRS) CTB–ED3	+	9.2 ± 0.36	0.239 ± 0.123
3	hRID–CTB–ED3	−	12.3 ± 0.51	0.2 ± 0.021
4	(hRID) CTB–ED3	+	8.2 ± 0.36	0.174 ± 0.003
5	NC–CTB–ED3	−	8.1 ± 0.63	0.338 ± 0.08
6	(NC) CTB–ED3	+	8.2 ± 0.28	0.253 ± 0.096
7	(NC) mCTB(Y12D)–ED3	+	8.5 ± 0.19	0.339 ± 0.021
8	(NC) mCTB(C9S)–ED3	+	7.8 ± 0.66	0.546 ± 0.125
9	(hRID) ED3	+	1.3 ± 0.27	0.256 ± 0.01

Note: The particle size (nm) and polydispersity index (PDI) values of each construct are presented with their corresponding margins of error. The table also indicates whether each construct was treated with TEV protease or left untreated.

Table 2. In most of the constructs, peak 2 is most prominent, which suggests that the majority of the monomers assembled into oligomers corresponding to the pentameric size, as designed.

In more detail, AsnRS-CTB-ED3 predominantly eluted in peak 2, which corresponds to the pentameric size (Figure 3a). SDS-PAGE analysis (right panel) confirmed the presence of oligomer-sized bands under non-reducing conditions (lane 2′, green arrow). After TEV cleavage, the majority of the proteins remained in peak 2 (Figure 3b, green arrow). Similarly, hRID-CTB-ED3 predominantly eluted in peak 2, which corresponds to the pentameric size, before and after TEV cleavage (Figure 3c,d). SDS-PAGE analysis (right panel) confirmed the presence of oligomer-sized bands (green arrow) under non-reducing conditions in peak 2. Following TEV cleavage, the proportion of proteins eluted in peak 1, which corresponds to aggregates, increased. However, the majority of the proteins remained in peak 2, where oligomer formation was abundantly observed by SDS-PAGE. In the case of NC-CTB-ED3, a stronger signal at peak 1 was exhibited compared to those of hRID-CTB-ED3 or AsnRS-CTB-ED3 (Figure 3e). SDS-PAGE results showed that, under non-reducing conditions, a portion of peak 1 displayed an oligomeric band (Figure 3e, green arrow). Peak 2 displayed a more prominent oligomer band (green arrow) in the SDS-PAGE. TEV cleavage was not efficient, and only ~40% of the protein underwent successful cleavage (Figure 3f, right panel, lane T). The cleaved form (black arrow) was more abundant in peak 2 than in peak 1.

The (NC) mCTB(Y12D)-ED3 and (NC) mCTB(C9S)-ED3 constructs that were designed to evaluate the receptor-binding and pentamer-forming abilities of CTB exhibited relatively low TEV cleavage efficiency (Figure 3g,h, lane T) compared with those of AsnRS or hRID-tag (Figure 3b,d, respectively). The Y12D variant maintained the oligomer structure, despite defects in the receptor GM1 binding (Figure 4). In contrast, the C9S variant failed to assemble into an oligomer (lack of peak 2, Figure 3h), thus confirming the importance of the intramolecular disulfide bonds in the assembly process (Jobling and Holmes 2002; Sung et al. 2024). Similar to the wild-type construct ((NC) CTB-ED3, (NC) mCTB(Y12D)-ED3) showed a greater proportion of the cleaved protein (black arrow) in peak 2 than in peak 1. Notably, (hRID) ED3 eluted predominantly in peak 3 (Figure 3i) as a monomer (lanes 3 and 3′ in SDS-PAGE), confirming that the CTB component is required as a scaffold for oligomer assembly. Overall, these findings provide critical insights into the structural properties and behaviour of these recombinant antigen proteins, as predicted in the design of sub-virion NPs (Figure S2a–f).

To further assess the size distribution of the SEC-purified fractions, DLS analysis was performed (Table 3, Figure S5a–i). All CTB-containing constructs, except for (hRID) ED3, exhibited hydrodynamic diameters within a similar size range, broadly compatible with the overall dimensions of the AlphaFold-predicted assemblies (Figure S2a–f). These DLS values were interpreted only as approximate indicators of particle size in solution and were not intended as direct geometric validation of the AlphaFold-predicted models. Notably, although (NC) mCTB(C9S)–ED3 showed a comparable average size, it displayed a substantially higher PDI, indicating a heterogeneous and non-uniform particle population.

3.4 | Structural Validation of CTB and ED3 Domains by GM1-Binding and E24-Binding ELISA

To evaluate the structural integrity of the recombinant antigens, ELISA assays were performed using GM1 ganglioside and

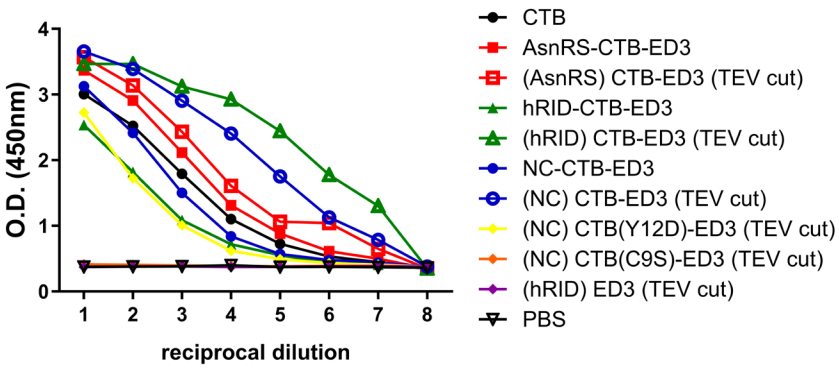

FIGURE 4 | GM1 ganglioside binding assay to assess the receptor binding capacity of the recombinant antigens. A GM1 binding assay was performed to compare the receptor-binding capacities of various recombinant antigens to the GM1 ganglioside. Commercial cholera toxin B subunit (CTB) was included as a positive control.

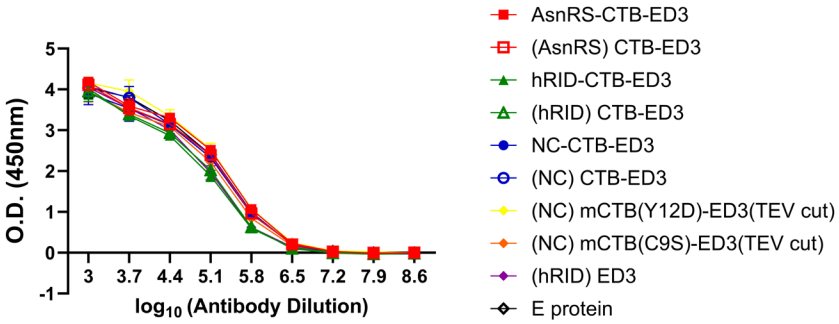

FIGURE 5 | E24-binding ELISA to assess the structural integrity of the ED3 domain in recombinant antigens. An E24-binding ELISA was performed to evaluate the structural integrity of the ED3 domain in the recombinant antigens. The E24 monoclonal antibody, which recognizes the lateral ridge epitope of WNV ED3, was used to assess antigenicity. Commercial WNV E protein was included as a positive control.

the ED3-specific monoclonal antibody E24 (Figures 4 and 5). GM1-binding analysis showed that, despite the differences in the origin and identity of the fusion tags, the TEV-cleaved forms of all constructs exhibited stronger GM1-binding activity than their uncleaved counterparts, likely due to the removal of the structural masking caused by the fusion tags. Wild-type CTB-containing recombinant antigen proteins revealed GM1-binding activity comparable to or higher than that of commercial CTB, except for hRID-CTB-ED3. In contrast, (NC) mCTB(Y12D)-ED3, which harbours a mutation that disrupts GM1 binding, exhibited markedly reduced binding compared to that of commercial CTB and (NC) CTB-ED3. In addition, (NC) mCTB(C9S)-ED3, which is unable to form a pentameric structure, showed negligible GM1-binding activity, comparable to that of the CTB-lacking ED3-only construct or PBS control. These results indicate that CTB fused to ED3 exhibits GM1-binding activity, consistent with the expected pentameric organization, and modulates the conformational and immunological quality of the recombinant antigen as expected for its role as a scaffold.

The structural integrity of the ED3 domain was further assessed using the E24 monoclonal antibody, which recognizes the lateral ridge epitope of WNV ED3, a major neutralizing epitope of the virus (Oliphant et al. 2005, 2006) (Figure 5). All ED3-containing constructs exhibited clear binding to E24, indicating that the ED3 domain retained this conformational epitope. Notably, the E24 binding profiles of the recombinant antigens were similar to that of the commercial WNV E protein used as a positive control. Together, these results indicate that both the CTB scaffold and the ED3 antigen maintained their structural integrity in the recombinant constructs.

3.5 | Visualization of Recombinant Antigen Particles by TEM

To verify the accuracy of the oligomeric peak observed in the SEC, TEM was performed. The assembly status of the protein was visualized, revealing nanoparticle structures (Figure 6). Each multimer containing the fusion tag exhibited dimensions of approximately 17 nm, while those without the fusion tag measured 11 nm (Figure 6a–g). As predicted, (NC) mCTB(Y-12D)-ED3 formed nanoparticle structures (Figure 6g), whereas (NC) mCTB(C9S)-ED3 was amorphous (Figure 6h), and (hRID) ED3 failed to exhibit any distinct structural features (Figure 6i). These results support the assembly of the recombinant protein into the nanoparticles, further extending the physicochemical properties examined by SDS-PAGE and SEC (Figure 3), and providing visual confirmation of the design of the recombinant vaccine.

3.6 | Immunogenicity of WNV ED3

To evaluate the overall antibody responses induced by each recombinant antigen, endpoint titres of total IgG were determined using mouse sera collected after immunization (Figure 7a). Among the fusion-tagged constructs, hRID–CTB–ED3 induced

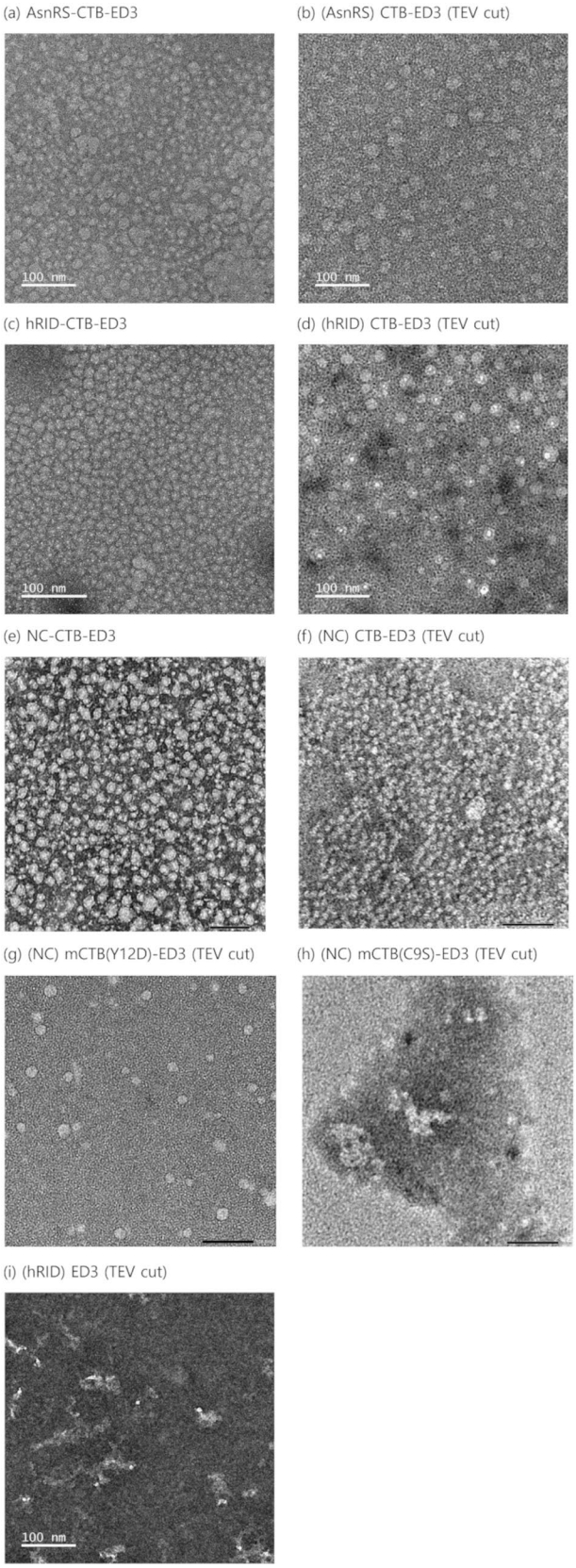

FIGURE 6 | Transmission electron microscopy (TEM) analysis of the recombinant antigens. TEM was performed on each construct, with images captured at a scale of 100 nm. (a) AsnRS-CTB-ED3, (b) (AsnRS) CTB-ED3, (c) hRID-CTB-ED3, (d) (hRID) CTB-ED3, (e) NC-CTB-ED3, (f) (NC) CTB-ED3, (g) (NC) mCTB(Y12D)-ED3, (h) (NC) mCTB(C9S)-ED3 and (i) (hRID) ED3.

significantly higher total IgG titres than AsnRS–CTB–ED3 and NC–CTB–ED3, whereas AsnRS–CTB–ED3 and NC–CTB–ED3 showed no significant difference. These results indicate that total IgG responses varied depending on the fusion tag used. Analysis of CTB variants revealed no significant differences among the wild-type CTB ((NC) CTB–ED3), the GM1-binding–defective construct ((NC) mCTB(Y12D)–ED3), and the pentamer-defective construct ((NC) mCTB(C9S)–ED3). The CTB-lacking (hRID) ED3 remained below the detection limit, suggesting that the CTB scaffold contributes to enhanced antibody responses. These results demonstrate that the *E. coli*–expressed antigenic proteins, when fused to CTB, effectively induced robust humoral immunity. To examine the Th2-associated antibody subclass, IgG1 titres were analysed (Figure 7b). Among the fusion-tagged constructs, hRID–CTB–ED3 elicited the highest response, showing significantly greater IgG1 titres than AsnRS–CTB–ED3 and NC–CTB–ED3. This indicates that the antibody response differed among the fusion-tagged constructs, with hRID–CTB–ED3 producing the strongest IgG1 response. Comparison among CTB variants revealed no significant differences among wild-type (NC) CTB–ED3, (NC) mCTB(Y12D)–ED3, and (NC) mCTB(C9S)–ED3. These findings indicate that IgG1 induction was primarily driven by the antigenic properties of the ED3 domain rather than by the oligomeric assembly or GM1-binding activity of CTB.

To assess the Th1-associated subclass, IgG2a titres were measured (Figure 7c). No significant differences were observed among the fusion-tagged constructs, indicating that the type of fusion tag did not influence IgG2a production. However, when comparing CTB variants, both (NC) CTB–ED3 and (NC) mCTB(Y12D)–ED3, which retain the ability to form pentamers, induced significantly higher IgG2a titres than (NC) mCTB(C9S)–ED3. Together, these findings indicate that IgG2a induction is governed primarily by the pentameric structural integrity of CTB rather than by the ED3 itself or the specific fusion tag used.

To evaluate the balance of immune responses, the ratio of IgG1 to IgG2a titres was calculated (Figure 7d). Values closer to 0 indicate a more balanced Th1/Th2 response, whereas higher and lower values reflect Th2- and Th1-biased responses, respectively. (NC) mCTB(C9S)-ED3 showed a marked IgG1 bias, whereas other CTB pentamer-competent constructs exhibited relatively balanced IgG1 and IgG2a responses. These results indicate that the recombinant antigens, which combine the nanoparticle-forming capability of CTB with the antigenic domain of ED3, elicited a well-balanced immune response encompassing both IgG1 and IgG2a subclasses.

To evaluate the virus-neutralizing activity of the recombinant antigens, a plaque reduction neutralization test (PRNT) was conducted using mouse sera collected after immunization (Figure 8). Neutralizing titres of each group were compared with those of (hRID) ED3 and the formalin-inactivated WNV to assess the presence and relative magnitude of neutralizing effects. When compared with the (hRID) ED3, hRID–CTB–ED3 and (NC) mCTB(Y12D)–ED3 exhibited significantly higher $PRNT_{50}$ titres, indicating that these particular CTB-fused constructs elicited stronger virus-neutralizing antibody responses than ED3 alone. When compared with the formalin-inactivated

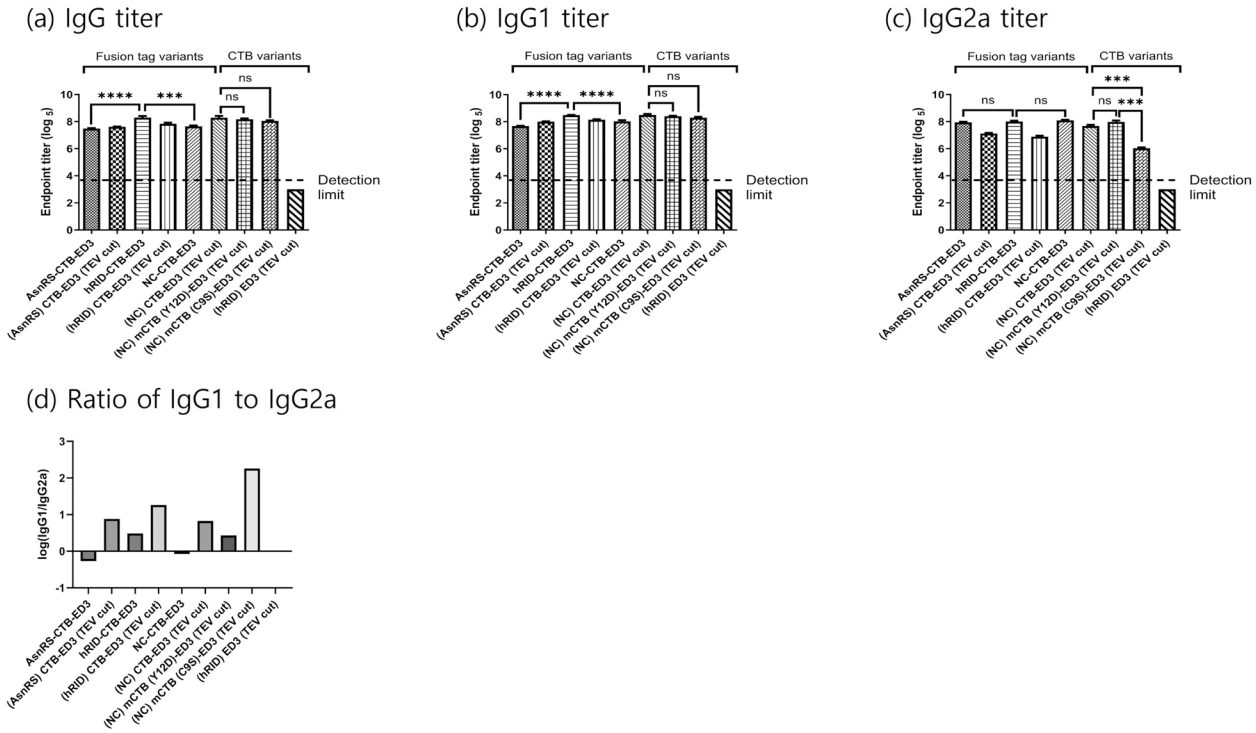

FIGURE 7 | Evaluation of the immunogenicity of the recombinant antigens in mice serum. Endpoint titres of (a) total IgG, (b) IgG1, and (c) IgG2a antibodies in mouse sera were determined by ELISA. Data are presented as the mean of three independent experiments, representing the humoral immune responses elicited by each antigen. (d) The IgG1/IgG2a ratio was calculated to assess the Th1/Th2 bias. The log-transformed ratio of IgG1 to IgG2a was used as an indicator of Th2 versus Th1 responses. Statistical significance was determined by one-way ANOVA followed by Tukey's multiple comparisons test. Asterisks denote statistical significance (*$p < 0.05$; **$p < 0.01$; ***$p < 0.001$); ns, not significant.

WNV group, (NC) mCTB(Y12D)–ED3 showed an even higher neutralizing activity. These findings demonstrate that the recombinant nanoparticle antigens containing the CTB scaffold effectively elicited neutralizing antibody responses in mice, and that the Y12D mutant, despite its loss of GM1-binding ability, achieved the strongest neutralizing capacity among the tested constructs.

3.7 | Cross-Reactivity of WNV ED3

To evaluate the potential cross-reactivity with other flaviviruses, the binding affinities of third-dose sera from WNV vaccine candidates were assessed using ELISA against representative flaviviruses (DENV, JEV, and ZIKV) (Figure 9a–c). The selected sera, hRID-CTB-WNV ED3, (NC) CTB-WNV ED3, and (NC) mCTB(Y12D)-WNV ED3, were chosen based on their relatively strong antibody titres (Figure 7a). Each serum sample was tested for its binding affinity to plates coated with live DENV, JEV, ZIKV, and inactivated WNV (Figure 9a–c). All three vaccine candidates exhibited strong binding to WNV, even at the lowest coating concentration (0.1 μg/well), whereas only minimal binding was observed against DENV, ZIKV, and JEV across all serum dilutions. In addition, increasing the coating concentration of WNV (0.1, 0.5, and 1 μg/well) resulted in progressively higher binding signals, indicating a concentration-dependent response. These results demonstrate that the recombinant nanoparticle antigens induce WNV-specific antibody responses with limited cross-reactivity to other flaviviruses.

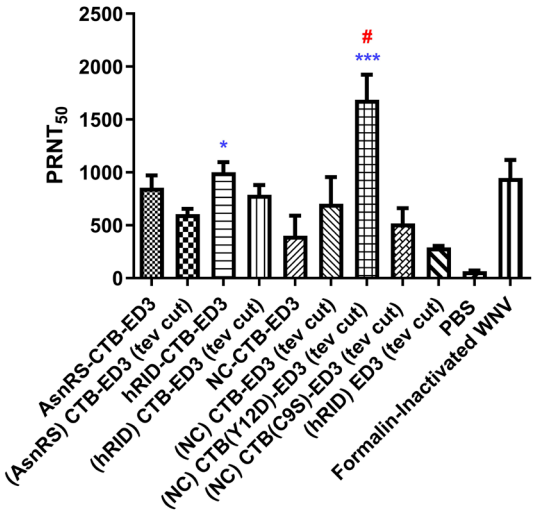

FIGURE 8 | Virus-neutralizing antibody responses induced by the recombinant antigens. The plaque reduction neutralization test (PRNT) results show the 50% neutralizing antibody titres ($PRNT_{50}$) in response to each antigen, highlighting the neutralizing efficacy of the immune response. Statistical significance was determined by one-way ANOVA followed by Dunnett's multiple comparisons test. Blue asterisks (*) indicate comparisons versus the (hRID) ED3 (TEV cut), and red hashes (#) indicate comparisons versus the Formalin-Inactivated WNV. Groups showing non-significant differences against both controls were not labelled for clarity. Significance levels: *, # $p < 0.05$; **, ## $p < 0.01$; ***, ### $p < 0.001$. Data on formalin-inactivated WNV were provided by the Korea Disease Control and Prevention Agency.

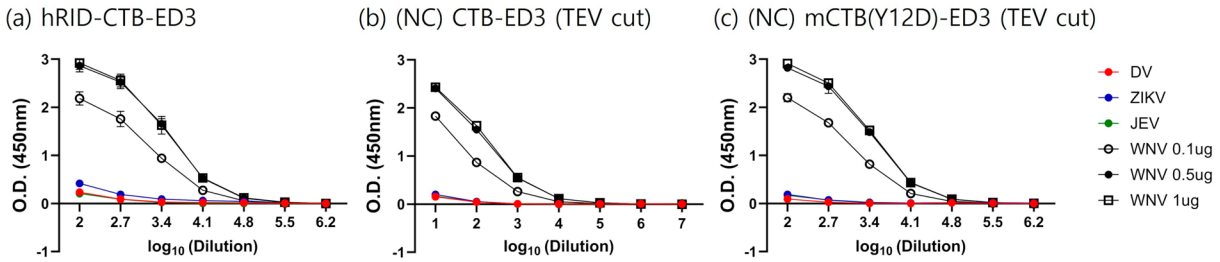

FIGURE 9 | Evaluation of the cross-reactivity potential of the sera from immunized mice. Cross-reactivity of sera from representative vaccine constructs (a) hRID-CTB-ED3, (b) (NC) CTB-ED3 (TEV cut), and (c) (NC) mCTB(Y12D)-ED3 (TEV cut) was evaluated.

4 | Discussion

An effective WNV vaccine should induce protective neutralizing antibody responses while limiting the generation of non-neutralizing antibodies associated with ADE (Bardina et al. 2017; Khan et al. 2021; Thomas et al. 2022). Although several candidates have reached Phase 1 or 2 clinical trials, none have progressed further, thus highlighting the complexity of WNV vaccine development (Ronca et al. 2021). Moreover, WNV research typically demands BSL-3 facilities, posing regulatory and safety concerns in manufacturing (Green and Ronca 2022). Therefore, there is a need for a novel vaccine strategy that can overcome these limitations, ensuring safety, efficacy, productivity, and regulatory concerns.

This study presents a recombinant WNV nanoparticle vaccine produced in *E. coli*. The vaccine design incorporates WNV ED3 fused with CTB, which functions as a structural scaffold and an immune-enhancer component (Hardy et al. 1988; Stratmann 2015). The recombinant antigens were successfully expressed and showed assembly behaviour consistent with nanoparticles, as confirmed by SDS-PAGE, SEC, and TEM analyses. Immunization studies in mice demonstrated robust humoral immune responses, including balanced Th1/Th2 immunity and the induction of neutralizing antibodies, along with limited cross-reactivity against other flaviviruses. As an alternative to cell-culture based virus production requiring high-level biosafety facilities, the present bacterially produced sub-virion nanoparticle would provide a robust and scalable strategy for developing recombinant vaccines against WNV and potentially other flaviviruses, amenable to large-scale production in BSL-2 facilities (Choi et al. 2009; Kim et al. 2020; Hwang et al. 2021; Lim et al. 2021).

Among the fusion-tagged constructs, hRID–CTB–ED3 consistently induced higher antibody titres than AsnRS–CTB–ED3 and NC–CTB–ED3, indicating that immunogenicity varied depending on the fusion tag used. Collectively, these findings demonstrate that the combination of CTB-mediated assembly and fusion tag selection enables efficient production of structurally assembled antigens with strong immunogenicity, supporting the feasibility of this bacterially produced nanoparticle platform for WNV vaccine development.

The contribution of CTB to the recombinant antigens was assessed through comparisons with mCTB variants and CTB-lacking ED3 constructs. The CTB-lacking (hRID) ED3 showed antibody responses below the detection limit, highlighting the essential contribution of CTB to immunogenicity. By contrast, the oligomeric constructs, (NC) CTB-ED3 and (NC) mCTB(Y12D)-ED3, exhibited similar IgG and IgG1 titres as those of the non-oligomeric (NC) mCTB(C9S)-ED3. However, in the case of IgG2a, the oligomeric constructs showed significantly higher titres than those of the non-oligomeric constructs. The IgG1/IgG2a ratio (Figure 7d) was markedly lower in the oligomeric constructs, thus indicating a more balanced Th1/Th2 response. These findings further support the immunomodulatory role of the nanoparticle structure of CTB in ensuring a balanced humoral immune profile. An unexpected finding was that (NC) mCTB(Y12D)-ED3, despite its reduced GM1 binding, exhibited the highest neutralization titres in the PRNT (Figure 8). This was surprising, as the Y12D mutation disrupts GM1 binding, which should theoretically reduce antigen uptake and immune response (Jobling and Holmes 2002). CTB normally binds GM1 on dendritic cells, macrophages, and B cells, thereby facilitating antigen presentation and T-cell activation (George-Chandy et al. 2001). It should be noted, however, that CTB acts as an immune stimulator and suppressor, depending on the context. CTB is a strong mucosal adjuvant, enhancing antigen-specific IgA and systemic antibody responses as a mucosal vaccine, whereas it can also induce immune tolerance when conjugated to an antigen and administered mucosally (Eriksson et al. 2003; Smits et al. 2009). Studies with GM1-binding mutants of CTB suggest that additional structural or signaling events beyond GM1 binding are required for integrated immune modulation (Aman et al. 2001). In the case of (NC) mCTB(Y12D)-ED3, the lack of GM1 binding suggests an alternative mechanism driving its strong neutralization response, which requires further investigation in the context of the versatility of CTB as an immunomodulatory agent.

Notably, recombinant WNV ED3-CTA2, a monomeric antigen fused with the toxic component of CT, was previously produced in *E. coli*, which showed a moderate level of production yield and immunogenicity (Tinker et al. 2014). The present CTB-ED3, purposefully designed as a multivalent assembly using a non-toxic component of CT as a scaffold, could be produced in high yields and elicit strong antibody responses. Although PRNT data were not available in the previous study for direct comparison, our findings suggest that the current CTB-based ED3 antigen, designed to present ED3 in a multivalent arrangement, elicited strong neutralizing antibody responses in mice. Given these advantages, the CTB-based assembly of sub-virion NP, as presented in this study, is expected to offer a promising option for the development of a WNV vaccine.

One limitation of this study is the absence of challenge data to directly assess the protective efficacy of the vaccine candidates,

which was partly due to limited access to BSL-3 containment. While the PRNT results provide a strong indication of the protective immune response, an in vivo challenge study would be necessary to confirm whether immunization effectively prevents WNV infection in animal models. Neutralizing antibody assays were based on infectious viruses in the present study, and a pseudovirus, if available in the near future, would greatly facilitate the testing of various vaccine candidates for preclinical development. In addition, as demonstrated by the mCTB(Y12D)-ED3 candidate, the relationship between GM1 receptor binding and the nature of the immunomodulatory function of the CTB component merits further investigation, particularly regarding antigen uptake, processing, and presentation into immune polarization.

This study highlights a promising WNV sub-virion nanoparticle vaccine that elicits balanced Th1 and Th2 responses, induces high neutralizing titres, and is amenable to low-cost production without requiring high-level biocontainment facilities. The in silico design of the CTB scaffold for the chimeric antigen can be translated into a practical production system, thereby enabling the highly regulated folding and assembly of the recombinant antigen. A similar design principle could be further extended to other flaviviruses and naked viruses with icosahedral assembly.

5 | Conclusion

This study presents a novel recombinant sub-virion nanoparticle vaccine candidate against WNV, featuring a CTB-based scaffold. The vaccine constructs demonstrated soluble expression, correct folding, and stable assembly in *E. coli*. Immunization studies in mice confirmed the robust and balanced Th1/Th2 immune responses, with neutralizing antibody titres that were comparable to those of formalin-inactivated antigens and exhibited no evidence of cross-reactivity. Notably, the nanoparticle configuration and specific fusion context played a crucial role in modulating immune polarization. CTB-based ED3 enabled the microbial production of chimeric antigen as a safe, scalable, and versatile strategy for WNV vaccine development, with possible applications to other flaviviruses that share similar structural topology.

Author Contributions

Sang-Mu Shim: investigation, resources, methodology. **Jung-Min Lee:** resources, investigation, methodology. **Jemin Sung:** conceptualization, methodology, investigation. **Hyun Byun:** conceptualization, investigation, writing – original draft, writing – review and editing, visualization, validation, methodology, formal analysis, data curation, project administration. **Seunghoo Kim:** resources. **Dah Hyun Moon:** resources. **Tae Hoon Kim:** conceptualization, investigation, writing – original draft, writing – review and editing, visualization, validation, methodology, formal analysis, project administration, data curation. **Sung Jae Kim:** resources. **Seong Hyun Park:** resources. **Hanul Kang:** investigation, methodology, resources. **Sin Hae Kang:** investigation, methodology, resources. **Doda Kim:** resources. **Gyoonhee Han:** supervision. **Baik Lin Seong:** supervision, writing – original draft, writing – review and editing.

Acknowledgements

We gratefully acknowledge the Korea Disease Control and Prevention Agency for providing inactivated WNV and support with the neutralization assays in the BSL-3 facilities under the National Institute of Health Funds (grant number: 2023-NI-015-00). This research was supported by the VITAL-Korea project funded by the Ministry of Health and Welfare of the South Korea (grant numbers: HV22C0259). Some schematic illustrations were created with the assistance of ChatGPT (OpenAI).

Funding

This work was supported by the Ministry of Health and Welfare of the South Korea, HV22C0259.

Ethics Statement

The authors have nothing to report.

Conflicts of Interest

The authors declare no conflicts of interest.

Data Availability Statement

The data that support the findings of this study are available within the article and its Supporting Information files. Additional data are available from the corresponding author upon reasonable request, subject to applicable institutional and biosafety restrictions.

References

Ahn, J., J. E. Yu, H. Kim, et al. 2023. "Ab5-Type Toxin as a Pentameric Scaffold in Recombinant Vaccines Against the Japanese Encephalitis Virus." *Toxins* 15, no. 7: 425.

Aman, A., S. Fraser, E. Merritt, et al. 2001. "A Mutant Cholera Toxin B Subunit That Binds GM1-Ganglioside but Lacks Immunomodulatory or Toxic Activity." *Proceedings of the National Academy of Sciences* 98, no. 15: 8536–8541.

Bachmann, M. F., and G. T. Jennings. 2010. "Vaccine Delivery: A Matter of Size, Geometry, Kinetics and Molecular Patterns." *Nature Reviews Immunology* 10, no. 11: 787–796.

Baldauf, K. J., J. M. Royal, K. T. Hamorsky, and N. Matoba. 2015. "Cholera Toxin B: One Subunit With Many Pharmaceutical Applications." *Toxins* 7, no. 3: 974–996.

Bardina, S. V., P. Bunduc, S. Tripathi, et al. 2017. "Enhancement of Zika Virus Pathogenesis by Preexisting Antiflavivirus Immunity." *Science* 356, no. 6334: 175–180.

Brandler, S., and F. Tangy. 2013. "Vaccines in Development Against West Nile Virus." *Viruses* 5, no. 10: 2384–2409.

Brinton, M. A. 2014. "Replication Cycle and Molecular Biology of the West Nile Virus." *Viruses* 6, no. 1: 13–53.

Choi, S. I., K. Ryu, and B. L. Seong. 2009. "RNA-Mediated Chaperone Type for de Novo Protein Folding." *RNA Biology* 6, no. 1: 21–24.

Chu, J. J. H., R. Rajamanonmani, J. Li, R. Bhuvanakantham, J. Lescar, and M. L. Ng. 2005. "Inhibition of West Nile Virus Entry by Using a Recombinant Domain III From the Envelope Glycoprotein." *Journal of General Virology* 86, no. Pt 2: 405–412.

Crill, W. D., and J. T. Roehrig. 2001. "Monoclonal Antibodies That Bind to Domain III of Dengue Virus E Glycoprotein Are the Most Efficient Blockers of Virus Adsorption to Vero Cells." *Journal of Virology* 75, no. 16: 7769–7773.

Curren, E. J., M. B. Shankar, M. Fischer, M. I. Meltzer, J. E. Staples, and C. V. Gould. 2021. "Cost-Effectiveness and Impact of a Targeted Age- and Incidence-Based West Nile Virus Vaccine Strategy." *Clinical Infectious Diseases* 73, no. 9: 1565–1570.

de Pinho Favaro, M. T., J. Atienza-Garriga, C. Martínez-Torró, et al. 2022. "Recombinant Vaccines in 2022: A Perspective From the Cell Factory." *Microbial Cell Factories* 21, no. 1: 203.

Eriksson, K., M. Fredriksson, I. Nordström, and J. Holmgren. 2003. "Cholera Toxin and Its B Subunit Promote Dendritic Cell Vaccination With Different Influences on Th1 and Th2 Development." *Infection and Immunity* 71, no. 4: 1740–1747.

Flores, H. E., E. F. Pinzon Burgos, S. Camacho Ortega, A. Heredia, and J. V. Chua. 2025. "From Antibodies to Immunity: Assessing Correlates of Flavivirus Protection and Cross-Reactivity." *Vaccine* 13, no. 5: 449.

George-Chandy, A., K. Eriksson, M. Lebens, I. Nordstrom, E. Schon, and J. Holmgren. 2001. "Cholera Toxin B Subunit as a Carrier Molecule Promotes Antigen Presentation and Increases CD40 and CD86 Expression on Antigen-Presenting Cells." *Infection and Immunity* 69, no. 9: 5716–5725.

Gill, D. M., and R. S. Rappaport. 1979. "Origin of the Enzymatically Active A1 Fragment of Cholera Toxin." *Journal of Infectious Diseases* 139, no. 6: 674–680.

Gould, C. V., J. E. Staples, C. Y.-H. Huang, A. C. Brault, and R. J. Nett. 2023. "Combating West Nile Virus Disease—Time to Revisit Vaccination." *New England Journal of Medicine* 388, no. 18: 1633–1636.

Green, F. M., and S. E. Ronca. 2022. "Safety Procedures to Work With West Nile Virus in Biosafety Level 3 Facilities." In *West Nile Virus: Methods and Protocols*, 205–210. Springer.

Hardy, S. J., J. Holmgren, S. Johansson, J. Sanchez, and T. R. Hirst. 1988. "Coordinated Assembly of Multisubunit Proteins: Oligomerization of Bacterial Enterotoxins In Vivo and In Vitro." *Proceedings of the National Academy of Sciences of the United States of America* 85, no. 19: 7109–7113.

Heinz, F., and K. Stiasny. 2012. "Flaviviruses and Their Antigenic Structure." *Journal of Clinical Virology* 55, no. 4: 289–295.

Holmgren, J., and I. Lönnroth. 1973. "Subunit Structure of Cholera Toxin." *Journal of General Microbiology* 76: 417–427.

Hwang, B. J., Y. Jang, S. B. Kwon, et al. 2021. "RNA-Assisted Self-Assembly of Monomeric Antigens Into Virus-Like Particles as a Recombinant Vaccine Platform." *Biomaterials* 269: 120650.

Jobling, M. G., and R. K. Holmes. 2002. "Mutational Analysis of Ganglioside GM1-Binding Ability, Pentamer Formation, and Epitopes of Cholera Toxin B (CTB) Subunits and CTB/Heat-Labile Enterotoxin B Subunit Chimeras." *Infection and Immunity* 70, no. 3: 1260–1271.

Kaiser, J. A., and A. D. T. Barrett. 2019. "Twenty Years of Progress Toward West Nile Virus Vaccine Development." *Viruses* 11, no. 9: 823.

Kanai, R., K. Kar, K. Anthony, et al. 2006. "Crystal Structure of West Nile Virus Envelope Glycoprotein Reveals Viral Surface Epitopes." *Journal of Virology* 80, no. 22: 11000–11008.

Kern, D., H. Roy, and H. D. Becker. 2013. "Asparaginyl-tRNA Synthetases." Madame Curie Bioscience Database [Internet], Landes Bioscience.

Khan, M. T., R. Islam, T. J. Jerin, et al. 2021. "Immunoinformatics and Molecular Dynamics Approaches: Next Generation Vaccine Design Against West Nile Virus." *PLoS One* 16, no. 6: e0253393.

Kim, Y. S., J. Lim, J. Sung, et al. 2020. "Built-In RNA-Mediated Chaperone (Chaperna) for Antigen Folding Tailored to Immunized Hosts." *Biotechnology and Bioengineering* 117, no. 7: 1990–2007.

Kuhn, R. J., W. Zhang, M. G. Rossmann, et al. 2002. "Structure of Dengue Virus: Implications for Flavivirus Organization, Maturation, and Fusion." *Cell* 108, no. 5: 717–725.

Kwon, S. B., J. E. Yu, C. Park, J. Lee, and B. L. Seong. 2018. "Nucleic Acid-Dependent Structural Transition of the Intrinsically Disordered N-Terminal Appended Domain of Human Lysyl-tRNA Synthetase." *International Journal of Molecular Sciences* 19, no. 10: 3016.

Lim, J., Y. Cheong, Y.-S. Kim, et al. 2021. "RNA-Dependent Assembly of Chimeric Antigen Nanoparticles as an Efficient H5N1 Pre-Pandemic Vaccine Platform." *Nanomedicine: Nanotechnology, Biology and Medicine* 37: 102438.

Lindenbach, B. D., and C. M. Rice. 2003. "Molecular Biology of Flaviviruses." *Advances in Virus Research* 59: 23–62.

Maiti, S., A. Singh, T. Maji, N. V. Saibo, and S. De. 2024. "Experimental Methods to Study the Structure and Dynamics of Intrinsically Disordered Regions in Proteins." *Current Research in Structural Biology* 7: 100138.

Mouhand, A., M. Pasi, M. Catala, et al. 2020. "Overview of the Nucleic-Acid Binding Properties of the HIV-1 Nucleocapsid Protein in Its Different Maturation States." *Viruses* 12, no. 10: 1109.

Moyle, P. M., and I. Toth. 2013. "Modern Subunit Vaccines: Development, Components, and Research Opportunities." *ChemMedChem* 8, no. 3: 360–376.

Mukhopadhyay, S., B.-S. Kim, P. R. Chipman, M. G. Rossmann, and R. J. Kuhn. 2003. "Structure of West Nile Virus." *Science* 302, no. 5643: 248.

Mukhopadhyay, S., R. J. Kuhn, and M. G. Rossmann. 2005. "A Structural Perspective of the Flavivirus Life Cycle." *Nature Reviews Microbiology* 3, no. 1: 13–22.

Oliphant, T., M. Engle, G. E. Nybakken, et al. 2005. "Development of a Humanized Monoclonal Antibody With Therapeutic Potential Against West Nile Virus." *Nature Medicine* 11, no. 5: 522–530.

Oliphant, T., G. E. Nybakken, M. Engle, et al. 2006. "Antibody Recognition and Neutralization Determinants on Domains I and II of West Nile Virus Envelope Protein." *Journal of Virology* 80, no. 24: 12149–12159.

Posadas-Herrera, G., S. Inoue, I. Fuke, et al. 2010. "Development and Evaluation of a Formalin-Inactivated West Nile Virus Vaccine (WN-VAX) for a Human Vaccine Candidate." *Vaccine* 28, no. 50: 7939–7946.

Rey, F. A., F. X. Heinz, C. Mandl, C. Kunz, and S. C. Harrison. 1995. "The Envelope Glycoprotein From Tick-Borne Encephalitis Virus at 2 Å Resolution." *Nature* 375, no. 6529: 291–298.

Ronca, S. E., J. C. Ruff, and K. O. Murray. 2021. "A 20-Year Historical Review of West Nile Virus Since Its Initial Emergence in North America: Has West Nile Virus Become a Neglected Tropical Disease?" *PLoS Neglected Tropical Diseases* 15, no. 5: e0009190.

Sanchez, J., and J. Holmgren. 2005. "Virulence Factors, Pathogenesis and Vaccine Protection in Cholera and ETEC Diarrhea." *Current Opinion in Immunology* 17, no. 4: 388–398.

Smits, H., A. Gloudemans, M. van Nimwegen, et al. 2009. "Cholera Toxin B Suppresses Allergic Inflammation Through Induction of Secretory IgA." *Mucosal Immunology* 2, no. 4: 331–339.

Some, D., H. Amartely, A. Tsadok, and M. Lebendiker. 2019. "Characterization of Proteins by Size-Exclusion Chromatography Coupled to Multi-Angle Light Scattering (SEC-MALS)." *Journal of Visualized Experiments* 148, no. 148: e59615.

Spohn, G., G. T. Jennings, B. E. Martina, et al. 2010. "A VLP-Based Vaccine Targeting Domain III of the West Nile Virus E Protein Protects From Lethal Infection in Mice." *Virology Journal* 7, no. 1: 146.

Stiasny, K., C. Kössl, J. Lepault, F. A. Rey, and F. X. Heinz. 2007. "Characterization of a Structural Intermediate of Flavivirus Membrane Fusion." *PLoS Pathogens* 3, no. 2: e20.

Stratmann, T. 2015. "Cholera Toxin Subunit B as Adjuvant—An Accelerator in Protective Immunity and a Break in Autoimmunity." *Vaccines (Basel)* 3, no. 3: 579–596.

Sun, H., D. Acharya, A. M. Paul, et al. 2023. "Antibody-Dependent Enhancement Activity of a Plant-Made Vaccine Against West Nile Virus." *Vaccine* 11, no. 2: 197.

Sung, J., Y. Cheong, Y. S. Kim, et al. 2024. "Harnessing Pentameric Scaffold of Cholera Toxin B (CTB) for Design of Subvirion Recombinant Dengue Virus Vaccine." *Vaccines (Basel)* 12, no. 1: 92.

Thomas, S., M. K. Smatti, A. Ouhtit, et al. 2022. "Antibody-Dependent Enhancement (ADE) and the Role of Complement System in Disease Pathogenesis." *Molecular Immunology* 152: 172–182.

Tinker, J. K., J. Yan, R. J. Knippel, P. Panayiotou, and K. A. Cornell. 2014. "Immunogenicity of a West Nile Virus DIII-Cholera Toxin A2/B Chimera After Intranasal Delivery." *Toxins* 6, no. 4: 1397–1418.

Wernick, N. L., D. J. Chinnapen, J. A. Cho, and W. I. Lencer. 2010. "Cholera Toxin: An Intracellular Journey Into the Cytosol by Way of the Endoplasmic Reticulum." *Toxins (Basel)* 2, no. 3: 310–325.

Zhang, Y., W. Zhang, S. Ogata, et al. 2004. "Conformational Changes of the Flavivirus E Glycoprotein." *Structure* 12, no. 9: 1607–1618.

Zhao, R., M. Wang, J. Cao, et al. 2021. "Flavivirus: From Structure to Therapeutics Development." *Life* 11, no. 7: 615.

Zlatkovic, J., K. Stiasny, and F. X. Heinz. 2011. "Immunodominance and Functional Activities of Antibody Responses to Inactivated West Nile Virus and Recombinant Subunit Vaccines in Mice." *Journal of Virology* 85, no. 5: 1994–2003.

Supporting Information

Additional supporting information can be found online in the Supporting Information section. **Figure S1:** Expression analysis of mCTB–WNV ED3 constructs with different fusion tags. SDS-PAGE analysis of recombinant mCTB–WNV ED3 constructs fused with different tags, including (a) AsnRS, (b) hRID, and (c) NC under non-induced (NI) and induced (I) conditions. Cell lysates were fractionated into total (T), soluble (S), and insoluble pellet (P) fractions. Non-reducing samples (S′) were prepared without boiling and DTT treatment to assess oligomer formation. Red boxes indicate bands corresponding to the monomeric form of the recombinant antigens, while green boxes indicate higher molecular weight species consistent with oligomeric assembly. **Figure S2:** Structural alignment and in silico 3D modelling of the monomeric and pentameric structures of the recombinant antigens. A 3D structural prediction was performed using AlphaFold 3. (a) Structural alignment of hRID-CTB-ED3 with the crystal structures of cholera toxin B subunit (CTB) (PDB ID: 1chq) and West Nile Virus (WNV) envelope protein domain III (ED3) (PDB ID: 1s6n) was conducted to verify the structural fidelity (green: 1chq, cyan: hRID-CTB-ED3 pentamer/monomer, purple: 1s6n). Among similarly predicted candidates, hRID-CTB-ED3 was selected as a representative model for comparative visualization. (b-e) All constructs were predicted to form stable pentameric structures, with diameters ranging from approximately 9 to 12 nm (bottom view). In these models, the fusion tag extends from the N-terminus of CTB, while the WNV ED3 domains are clustered at the C-terminus. (f) NC-mCTB(C9S)-ED3 monomer is shown with its measured size. (b) AsnRS-CTB-ED3; (c) hRID-CTB-ED3; (d) NC-CTB-ED3; (e) NC-mCTB(Y12D)-ED3; and (f) NC-mCTB(C9S)-ED3 (blue: CTB, green: ED3, red: AsnRS, yellow: hRID, purple: NC, cyan: mCTB(Y12D), orange: mCTB(C9S)). **Figure S3:** SDS-PAGE analysis of the purification of recombinant antigens. SDS-PAGE analysis of the constructs following Ni-affinity chromatography: (a) AsnRS-CTB-ED3; (b) hRID-CTB-ED3; (c) NC-CTB-ED3; (d) NC-mCTB(Y12D)-ED3; (e) NC-mCTB(C9S)-ED3; and (h) hRID-ED3. All constructs showed elution of recombinant proteins corresponding to the increased imidazole concentration. Elution was performed using a 10–100% buffer B gradient for hRID- and AsnRS-fused proteins, and a 20–100% buffer B gradient for NC-fused proteins. Non-reducing samples were loaded at the far right to demonstrate the formation of oligomeric structures. T, supernatant of lysed cell; M, molecular weight marker; number, fraction number; number', fraction under non-reducing conditions without DTT and boiling. **Figure S4:** Calibration of size-exclusion chromatography using molecular weight standards. Size-exclusion chromatography (SEC) calibration profile generated using protein standards of known molecular weights, including thyroglobulin (660 kDa), ferritin (440 kDa), aldolase (158 kDa), and ovalbumin (43 kDa). **Figure S5:** Dynamic Light Scattering (DLS) Analysis. Dynamic light scattering (DLS; Nano-ZS, Malvern Instruments, UK) was performed to analyse the size distribution of nanoparticles eluted from size exclusion chromatography (SEC). (a) AsnRS-CTB-ED3, (b) (AsnRS) CTB-ED3, (c) hRID-CTB-ED3, (d) (hRID) CTB-ED3, (e) NC-CTB-ED3, (f) (NC) CTB-ED3, (g) (NC)mCTB(Y12D)-ED3, (h) (NC)mCTB(C9S)-ED3, and (i) (hRID) ED3. The size distributions of each construct are shown in the corresponding graphs and summarized in the table below. All samples were measured in triplicate at 25°C.